A molecular mechanism directly linking E-cadherin adhesion to initiation of epithelial cell surface polarity

Lene N. Nejsum and W. James Nelson

Department of Biological Sciences and Department of Molecular and Cellular Physiology, The James H. Clark Center, Bio-X Program, Stanford University, Stanford, CA 94305

Mechanisms involved in maintaining plasma membrane domains in fully polarized epithelial cells are known, but when and how directed protein sorting and trafficking occur to initiate cell surface polarity are not. We tested whether establishment of the basolateral membrane domain and E-cadherin–mediated epithelial cell–cell adhesion are mechanistically linked. We show that the basolateral membrane aquaporin (AQP)-3, but not the equivalent apical membrane AQP5, is delivered in post-Golgi structures directly to forming cell–cell contacts where it co-accumulates precisely with E-cadherin. Functional disruption of individual components of a putative lateral targeting patch (e.g., microtubules, the exocyst, and soluble *N*-ethylmaleimide–sensitive factor attachment protein receptors) did not inhibit cell–cell adhesion or colocalization of the other components with E-cadherin, but each blocked AQP3 delivery to forming cell–cell contacts. Thus, components of the lateral targeting patch localize independently of each other to cell–cell contacts but collectively function as a holocomplex to specify basolateral vesicle delivery to nascent cell–cell contacts and immediately initiate cell surface polarity.

Introduction

The asymmetric distribution of membrane proteins in different cell surface domains is a feature common to many types of polarized cells, including epithelia, neurons, and immune cells (Yamada and Nelson, 2007). In epithelial cells, membrane proteins are segregated into functionally and structurally different apical and basolateral membrane domains. Considerable evidence has accumulated that the Golgi complex (Rodriguez-Boulan and Musch, 2005) and the recycling endosome (Ang et al., 2004) regulate sorting of apical and basolateral membrane proteins into separate vesicles in the exocytic and endocytic (recycling) pathways. However, less is known about mechanisms that specify post-Golgi vesicle delivery and fusion with the correct membrane domain.

Correspondence to W. James Nelson: wjnelson@stanford.edu; or Lene N. Nejsum: nejsum@stanford.edu

Abbreviations used in this paper: AQP, aquaporin; FLIP, fluorescence loss in photobleaching; PAGFP, photoactivated GFP; tdRFP, tandem-dimer red fluorescent protein; TIRF, total internal reflection fluorescent; t-SNARE and v-SNARE, target- and vesicle-soluble *N*-ethylmaleimide–sensitive factor attachment protein receptor, respectively.

The online version of this article contains supplemental material.

In fully polarized cells, the delivery of basolateral membrane proteins from the TGN and recycling endosomes to the plasma membrane may be regulated at several steps, including long-range vesicle delivery and membrane tethering and fusion. Vesicles travel from the region of the TGN to the plasma membrane along microtubules (Wacker et al., 1997). Upon arrival at the plasma membrane, vesicles are thought to interact with the exocyst (Sec6/8 complex; Guo and Novick, 2004) which is a multiprotein complex that may tether vesicles to the membrane before their fusion by a complex of vesicle-soluble *N*-ethylmaleimide–sensitive factor attachment protein receptors (v-SNAREs) and target (t)-SNAREs (Chen and Scheller, 2001; Brunger, 2005). In fully polarized MDCK cells, the exocyst is localized to the apex of the lateral membrane, and addition of function-blocking Sec8 antibodies inhibited basolateral, but not apical, vesicle delivery to the plasma membrane (Grindstaff et al., 1998b). In these cells, the t-SNARE syntaxin 4 is also localized to the basolateral plasma membrane (Li et al., 2002), and inhibition of t-SNARE function using botulinum neurotoxins blocked basolateral vesicle delivery (Ikonen et al., 1995). It has been suggested that the exocyst and t-SNAREs compose

The Journal of Cell Biology, Vol. 178, No. 2, July 16, 2007 323–335
http://www.jcb.org/cgi/doi/10.1083/jcb.200705094

a vesicle "targeting patch" that specifies basolateral vesicle delivery to sites of cell–cell adhesion (Drubin and Nelson, 1996), but this hypothesis has never been directly tested.

Cell adhesion to other cells and the extracellular matrix is important in the generation of epithelial cell surface polarity. In nonpolarized fibroblasts (Yoshimori et al., 1996) and single MDCK cells grown in suspension culture in the absence of cell contacts (Wang et al., 1990), apical and basolateral membrane proteins are intermixed on the cell surface, though they are sorted from each other in the exocytic pathway. Upon cadherin-mediated cell–cell adhesion in fibroblasts (McNeill et al., 1990) and suspension-grown MDCK cells (Wang et al., 1990), basolateral membrane proteins are restricted to cell–cell contacts, whereas apical proteins accumulate on the unbounded membrane facing the growth medium. Cell–cell adhesion is also critical for the correct orientation of asymmetric cell divisions in the stem cells and maintenance of the stem cell–niche interface (Song et al., 2002; Lechler and Fuchs, 2005; Siegrist and Doe, 2006). Adhesion to the extracellular matrix also plays a role in cell polarization, as laminin is required for correct apical pole orientation in three-dimensional epithelial cysts (O'Brien et al., 2001) and induces β-casein secretion from single mammary epithelial cells (Streuli et al., 1991). Although these studies are suggestive of a role for extracellular contacts in the orientation of different membrane domains in fully polarized cells, a link between these spatial cues and localized vesicle delivery, and the mechanisms involved have not been investigated directly.

We have taken a direct approach to these problems by examining the distributions of aquaporins (AQP) during initial cell–cell adhesion in MDCK cells. AQPs are a structurally homologous family of channel proteins that facilitate the movement of water, glycerol, and urea across different membrane domains in polarized epithelia. AQP3 has an N-terminal basolateral sorting signal (Rai et al., 2006) and localizes to the basolateral membrane in multiple epithelial tissues (Frigeri et al., 1995), whereas AQP5 has a C-terminal signal for targeting to or retention in the apical membrane (Wellner et al., 2005) and localizes to the apical membrane of secretory tissues (He et al., 1997; Nejsum et al., 2002) . We show that post-Golgi vesicles containing AQP3, but not AQP5, are targeted directly to the site of initial E-cadherin–mediated cell–cell contacts. Components of a putative lateral targeting patch localize rapidly and independently of each other to sites of cell–cell adhesion, where they function as a holocomplex that specifies basolateral vesicle delivery to cell–cell contacts. These results have broad implications for how cell polarity may be initiated by extrinsic spatial cues in a wide variety of differentiated and stem cells.

Results

Basolateral AQP3 accumulates with E-cadherin precisely at the site of initial cell–cell adhesion

Protein distributions during cell–cell adhesion were examined by high resolution time-lapse imaging in MDCK cells cotransfected with tandem-dimer red fluorescent protein (tdRFP)–tagged E-cadherin and either EGFP-tagged AQP3 or EGFP-tagged AQP5. EGFP-tagged forms of E-cadherin (Adams et al., 1998), AQP3, and AQP5 (Zelenina et al., 2003; Fig. 1 A) localize correctly. Note that the expression of tagged forms of E-cadherin did not increase overall levels of E-cadherin in cells because of a decrease in the level of endogenous E-cadherin commensurate with the level of ectopic E-cadherin (Adams et al., 1998).

E-cadherin rapidly accumulated at sites of initial cell–cell adhesion and spread laterally as the surface area of the contact increased (Fig. 1, B and C; Video 1, right; and Video 2, right, available at http://www.jcb.org/cgi/content/full/jcb.200705094/DC1), as reported previously (Adams et al., 1998). Shortly after the accumulation of E-cadherin was detected at the cell–cell contact, increased levels of AQP3 were detected at the same locations (Fig. 1 B; and Video 1, left). Thereafter, the accumulation of AQP3 was strikingly coincident with that of E-cadherin at all times during cell–cell adhesion. During final compaction of the cell–cell contact, the brightest regions of AQP3 were superimposed onto plaques of E-cadherin that coalesced at the edges of the cell–cell contact. Although some AQP5 (Fig. 1 C; and Video 2, left) was detected at the cell–cell contact with E-cadherin (Fig. 1 C; and Video 2, right) at the beginning of the time-lapse imaging, it rapidly disappeared, and as the cell–cell contact spread, AQP5 remained diffusely distributed over the entire surface and did not accumulate at the cell–cell contact. Quantitation confirmed that AQP3, but not AQP5, accumulated at cell–cell contacts (Fig. 1 D). Collectively, these results demonstrate that a basolateral protein AQP3, but not a homologous apical protein AQP5, precisely coaccumulated with E-cadherin during the very earliest stages of cell–cell adhesion.

Although both AQP3 and AQP5 are normally expressed in polarized epithelial cells, we tested whether the difference in localization of ectopic AQP3 and AQP5 to nascent cell–cell contacts was the same as that of endogenous basolateral and apical membrane proteins in MDCK cells. We plated cells at low density, fixed them after 1 h when initial cell–cell contacts had formed, and stained for two endogenous membrane proteins: the basolateral membrane protein NaK-ATPase and the apical membrane protein gp135 (podocalyxin; Fig. 1, E and F). NaK-ATPase (Fig. 1 E), like AQP3 (Fig. 1 B; and Video 1, left), accumulated precisely with E-cadherin at the cell–cell contact. On the other hand, gp135 (Fig. 1 F), like AQP5 (Fig. 1 C; and Video 2, left), did not accumulate at cell–cell contacts and was diffusely distributed over the cell surface. Hence, both exogenously expressed basolateral AQP3 (Fig. 1 B; and Video 1, left) and endogenously expressed NaK-ATPase (Fig. 1 E) coaccumulated with E-cadherin at cell–cell contacts, whereas apical AQP5 (Fig. 1 C; and Video 2, left) and gp135 (Fig. 1 F) did not.

Newly synthesized AQP3 is targeted directly to the site of E-cadherin–mediated cell–cell adhesion

Protein accumulation at nascent cell–cell contacts is dependent on the balance between delivery from intracellular compartments and lateral diffusion in the plasma membrane. We initially designed experiments to directly observe delivery of newly synthesized AQP3 from the Golgi (Fig. 2 A; and Video 3, left, available

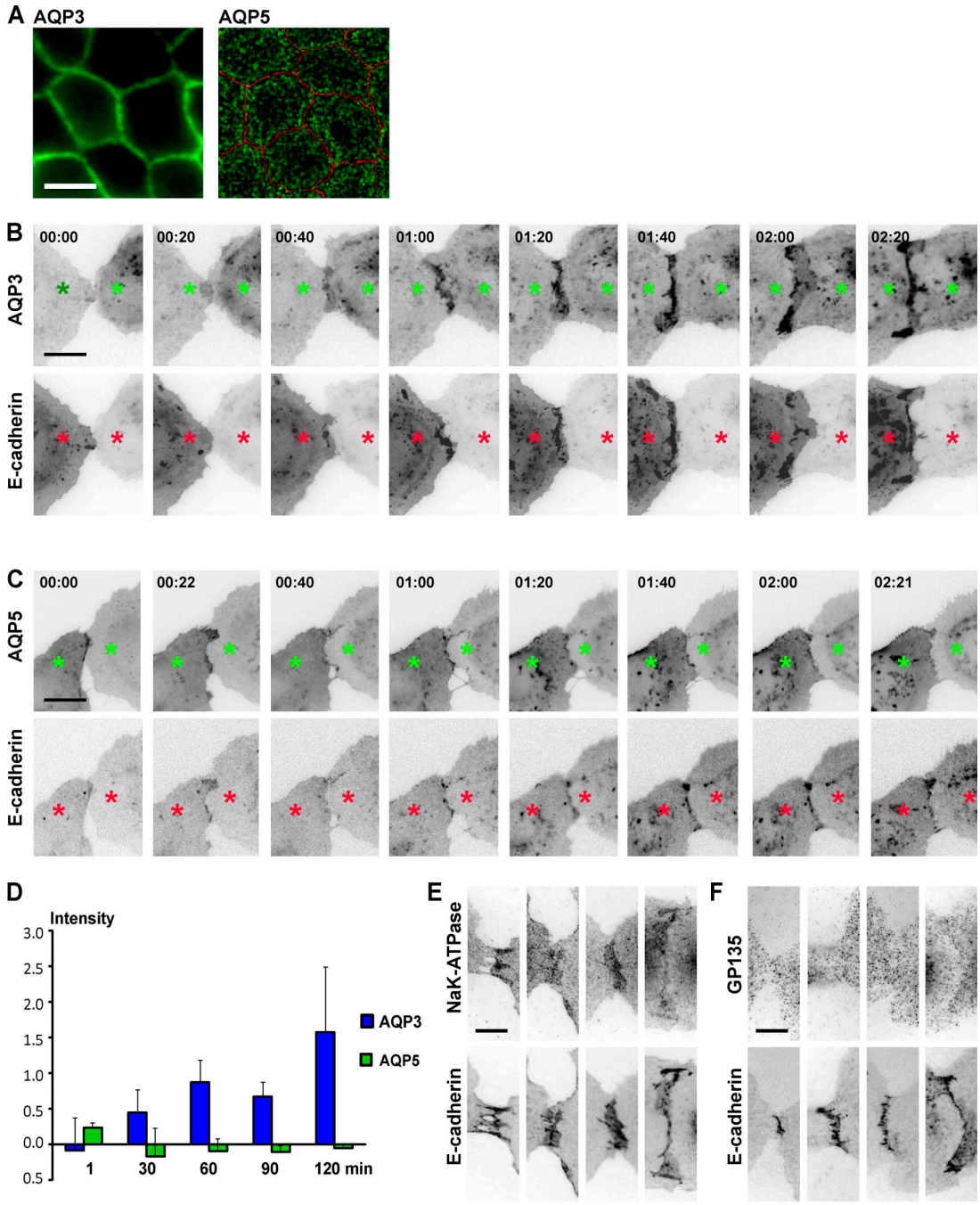

Figure 1. **AQP3 and AQP5 distributions upon initial cell–cell adhesion.** (A) Polarized MDCK cells grown on filters stably expressing AQP3-EGFP and AQP5-EGFP (green) and immunostained for ZO-1 (red). AQP3-EGFP localizes to the basolateral membrane, and AQP5-EGFP localizes to the apical membrane. Bar, 10 μm. (B and C) Representative examples of frames from time-lapse imaging of initial cell–cell adhesion of cells expressing tdRFP-labeled E-cadherin and either EGFP-labeled AQP3 (B) or EGFP-labeled AQP5 (C). Images were captured every minute. E-cadherin–tdRFP accumulates at cell–cell contacts, and AQP3-EGFP coaccumulates with E-cadherin–tdRFP. Some AQP5-EGFP is at the contact at the beginning of cell–cell adhesion, but it disappears from the contact and does not coaccumulate with E-cadherin–tdRFP. Asterisks indicate a single cells. Numbers indicate the time (in minutes) after the start of the time-lapse movie. Bars, 10 μm. (D). Quantitation of AQP3 and AQP5 accumulation at cell–cell contacts. Data points are averages of three independent experiments, and the error bars represent the SEM. Time (in minutes) is depicted on the x axis. (E) E-cadherin–tdRFP–expressing cells forming contacts and immunostained for NaK-ATPase and gp135. The basolateral NaK-ATPase colocalized with E-cadherin at all stages of contact formation. Apical gp135 does not localize to cell–cell contacts. Bar, 5 μm. See Videos 1 and 2, available at http://www.jcb.org/cgi/content/full/jcb.200705094/DC1.

at http://www.jcb.org/cgi/content/full/jcb.200705094/DC1). We created a stable cell line expressing AQP3 tagged with photoactivated GFP (AQP3-PAGFP), which allowed us to activate a small intracellular pool of AQP3-PAGFP in the Golgi and follow its fate by time-lapse imaging in a blank background; note that the signal from the EGFP-tagged protein is too bright at cell–cell contacts to allow visualization of increased accumulation after release of protein from the Golgi.

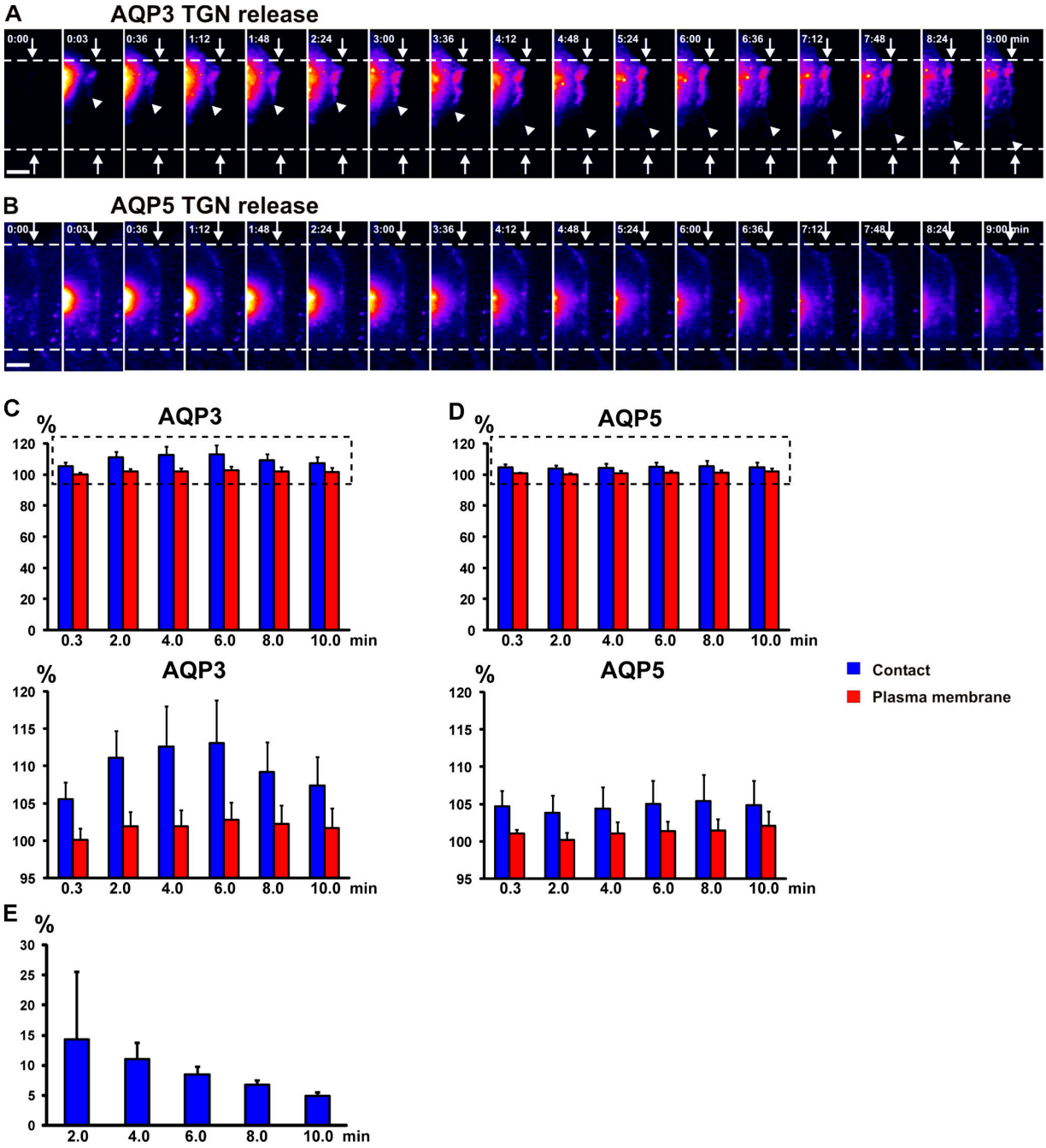

Figure 2. **AQP3, not AQP5, is delivered from the Golgi to cell–cell contacts.** (A and B) Representative example of release from a 19°C block of Golgi-accumulated AQP3-PAGFP (A; see Fig. 7 A) and AQP5-PAGFP (B) in pairs of adhering cells. AQP3-PAGFP rapidly accumulates at cell–cell contacts after photoactivation in the Golgi (A), whereas AQP5-PAGFP does not (B). Arrowheads in A point to the edge of AQP3-PAGFP accumulation, arrows point to the edge of cell–cell contacts, and numbers indicate the time (in minutes) after activation. The fluorescence intensity scale is pseudocolored. Bars, 5 μm. (C and D) Quantitation over time of a small spot of AQP3-PAGFP and AQP5-PAGFP fluorescence at the cell–cell contact proximal to the Golgi (blue, fluorescence intensity at cell–cell contacts; red, fluorescence intensity at the plasma membrane as equidistant from the Golgi as the spot measured at the cell–cell contact). Data points are averages of five independent experiments, and the error bars represent the SEM. The dashed boxes (top) indicate the insets shown (bottom). Quantitation shows that AQP3-PAGFP (C) accumulates at cell–cell contact, whereas AQP5-PAGFP (D) does not. Numbers indicate the time (in minutes) after activation. (E) Quantitation of the increase in AQP3-PAGFP fluorescence at cell–cell contacts relative to fluorescence loss of AQP3-PAGFP from the Golgi after release from a 19°C block. Quantitation shows that 2 min after release, 15% of the loss of AQP3-PAGFP fluorescence from the Golgi accumulates at cell–cell contact. Data points are averages of five independent experiments, and the error bars represent the SEM. Time (in minutes) is depicted on the x axis. See Video 3, available at http://www.jcb.org/cgi/content/full/jcb.200705094/DC1.

To synchronize cell surface delivery of protein, AQP3-PAGFP was accumulated in the Golgi by a 19°C block and released by shifting to 37°C. Although photoactivation of AQP3-PAGFP at the Golgi could activate AQP3-PAGFP in other membrane compartments localized close to the Golgi (e.g., endosomes), it has been shown that the 19°C block causes the accumulation of newly synthesized protein in the TGN (Pfeiffer et al., 1985). A spot of AQP3-PAGFP over the Golgi was laser activated and

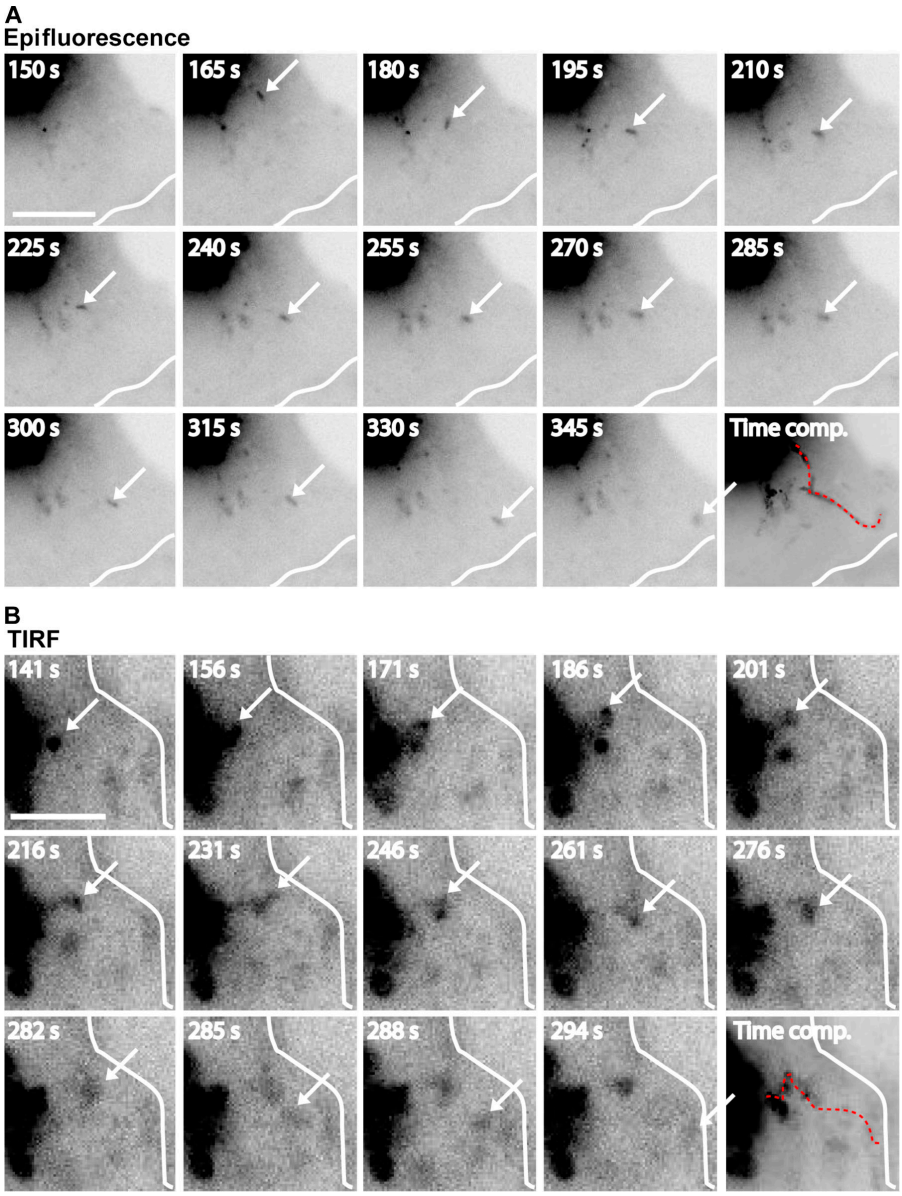

Figure 3. **AQP3-PAGFP post-Golgi carriers traffic to cell–cell contacts.** (A and B) Post-Golgi carriers containing AQP3-PAGFP travel from the Golgi to the cell–cell contact (white line) after release from a 19°C block. The carriers (arrows) were followed by epifluorescence (A) and TIRF (B) microscopy. Time-composite images show the trajectories (red dotted lines) of individual carriers from the Golgi to the cell–cell contact. Numbers indicate the time (in seconds) after photoactivation. Bars, 5 μm. See Videos 4–6, available at http://www.jcb.org/cgi/content/full/jcb.200705094/DC1.

followed by time-lapse imaging for a short period (<10 min) in pairs of cells forming cell–cell contacts (Fig. 2 A; Video 3, left; and see Fig. 7 A). The intensity of the activated pool of AQP3-PAGFP decreased rapidly around the Golgi, and after a short delay (<1 min), there was a concomitant increase in AQP3-PAGFP at the cell– cell contact; note that AQP3-PAGFP initially accumulated at the membrane immediately adjacent to the activated spot in the Golgi and then more distally during later times. We quantified the fluorescent intensities of equal areas of AQP3-PAGFP at the cell–cell contact (Fig. 2 C, blue) and at the noncontacting plasma membrane (Fig. 2 C, red) that were equidistant from the initial photoactivated spot. The intensity of AQP3-PAGFP fluorescence increased in the cytosol (not depicted) and at the site of cell–cell adhesion (Fig. 2 C, blue) but not at the noncontacting plasma membrane (Fig. 2 C, red); this is consistent with direct delivery of AQP3-PAGFP from the Golgi to the site of initial cell–cell contact. In contrast to AQP3-PAGFP, we found that AQP5-PAGFP activated in the Golgi did not accumulate at the site of cell–cell adhesion (Fig. 2, B and D; and Video 3, right).

Individual post-Golgi carriers could be observed leaving the initial region of AQP3-PAGFP activation in the direction of the site of initial cell–cell contact and traveled all the way to the contact, where they disappeared (Fig. 3; Video 4; and Video 5, available at http://www.jcb.org/cgi/content/full/jcb.200705094/DC1). These vesicles were observed by either epifluorescence microscopy (Fig. 3 A and Video 4) or total internal reflection fluorescent (TIRF) microscopy (Fig. 3 B and Video 5). Because the volume of cytoplasm in thin lamellipodia forming cell–cell contacts is low, it is likely that the disappearance of these vesicles is a consequence of their fusion with the plasma membrane rather than their diffusion out of the focal plane. These post-Golgi carriers traveled in linear paths, with several pauses and changes of direction (Fig. 3, A and B; Video 4; and Video 5), at speeds averaging 0.2–0.3 μm/s, which correlates well with vesicle movements generated by the microtubule motor kinesin

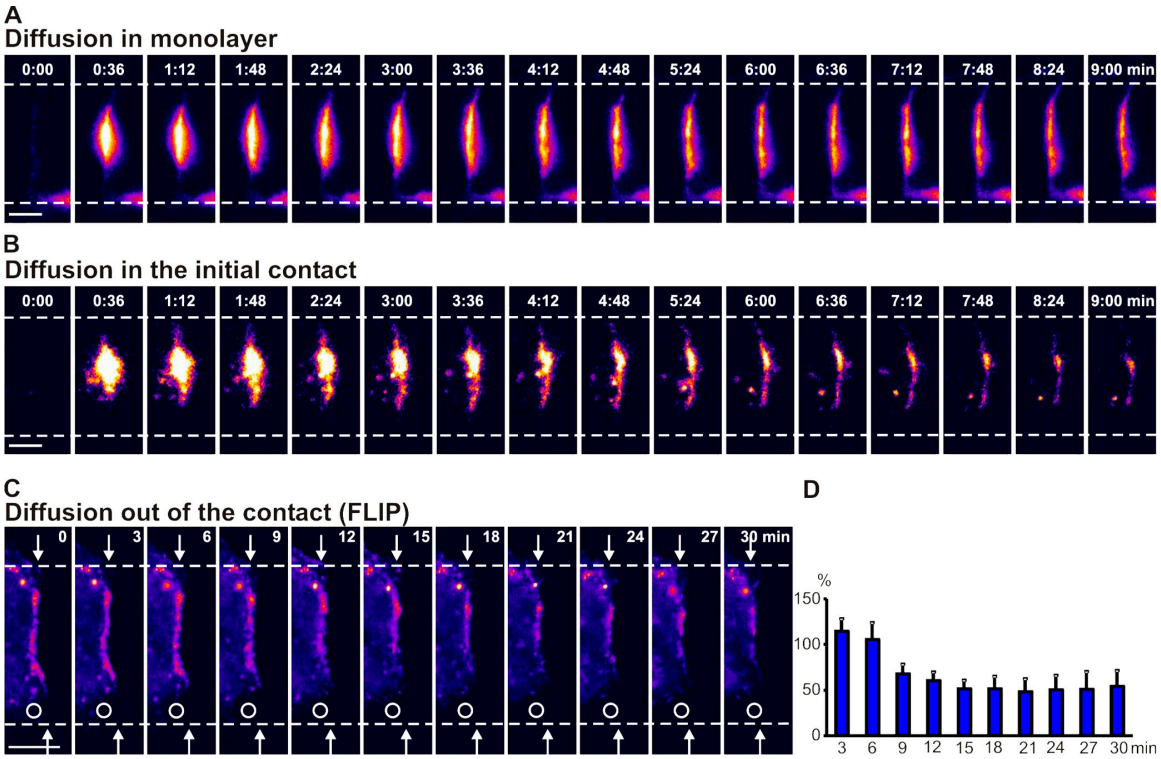

Figure 4. **AQP3-PAGFP diffusion at cell–cell contacts.** (A and B) Diffusion of AQP3-PAGFP activated at cell–cell contacts in 24-h monolayers (A) or initial cell pairs (B). Diffusion is very rapid at cell–cell contacts of a cell pair ($t_{1/2}$ = 19 ± 8 s; B) compared with 24-h monolayers of cells ($t_{1/2}$ = 143 ± 46 s; A). The fluorescence intensity scale is pseudocolored, and the time is shown (in minutes). Data points are averages of eight independent experiments, and error bars represent the SEM. Bars, 5 μm. (C) FLIP experiment. Continuous photobleaching (open circles) of the plasma membrane adjacent to the cell–cell contact in a pair of cells of which one cell is expressing AQP3-EGFP and the other is a nonexpressing cell. AQP3-EGFP rapidly diffuses out of the contact. Arrows point to the edge of the cell–cell contact. Time is shown (in minutes). The fluorescence intensity scale is pseudocolored. Bar, 10 μm. (D) Quantitation over time of a small spot of AQP3-EGFP at the cell–cell contact adjacent to the site of continuous photobleaching (FLIP) after background subtraction. Data points are averages of three independent experiments, and the error bars represent the SEM. Time (in minutes) is depicted on the x axis.

(Hua et al., 1997). Approximately 15% of the loss of AQP3-PAGFP fluorescence in the Golgi was detected at the cell–cell contact after 2 min (Fig. 2 E). This correlates well with measurements by cell surface biotinylation that 20% of the low density lipoprotein receptor was delivered from the Golgi to the plasma membrane after release from a 19°C block in polarized MDCK cells (Grindstaff et al., 1998b). We conclude that basolateral membrane AQP3, but not the equivalent apical membrane AQP5, is targeted directly from the Golgi to initial sites of E-cadherin–mediated cell–cell adhesion.

Rapid membrane diffusion of AQP3 at cell–cell contacts

Although the results described in the previous paragraph show direct delivery of AQP3 from the Golgi to cell–cell contacts, protein accumulation could also be affected by diffusion between the noncontacting plasma membrane and the cell–cell contact. To measure protein diffusion, AQP3-PAGFP was activated in a small spot within the cell–cell contact (Fig. 4, A and B; and Video 6, available at http://www.jcb.org/cgi/content/full/jcb.200705094/DC1), and the fluorescence intensity of the spot was measured over time. The diffusion coefficient of AQP3 was fast at initial contacts between cell pairs ($t_{1/2}$ = 19 ± 8 s; Fig. 4 B; and Video 6, right); for comparison, we measured AQP3 diffusion in confluent monolayers that had begun to establish full polarity over a period of 24 h and found that AQP3 diffusion was slower ($t_{1/2}$ = 143 ± 46 s; Fig. 4 A; and Video 6, left), indicating a change in AQP3 organization in the membrane during development of cell polarity. To test if AQP3 was retained at the contact or was free to diffuse into the noncontacting plasma membrane, we performed fluorescence loss in photobleaching (FLIP) of AQP3-EGFP at the plasma membrane adjacent to the contact (Fig. 4 C). In this experiment, MDCK cells stably expressing AQP3-EGFP were mixed with nonexpressing cells to examine protein diffusion in only one membrane of the cell pair at the cell–cell contact and in the presence of cyclohexamide to eliminate the addition of newly synthesized protein to the plasma membrane. The intensity of a small spot of fluorescence at the contact was quantitated over time and showed that AQP3-EGFP fluorescence dissipated rapidly (Fig. 4 D), consistent with rapid diffusion within the contact and the surrounding noncontacting plasma membrane. Collectively, these results show that AQP3 diffuses rapidly in the plane of the membrane and, hence, accumulation of AQP3 at cell–cell contacts must require rapid, direct, and sustained delivery of AQP3 from the Golgi.

Components of the lateral targeting patch localize to nascent cell–cell contacts

We tested whether components of the putative lateral targeting patch, consisting of the exocyst and SNARE complexes,

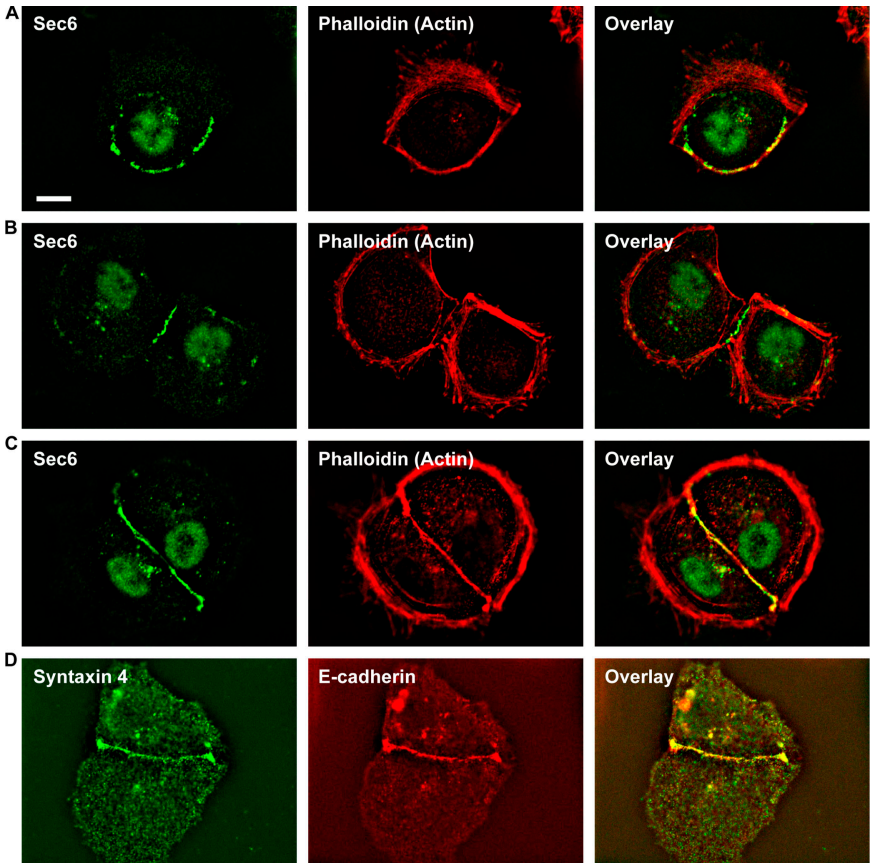

Figure 5. **The exocyst and Syntaxin 4 localize to initial cell–cell contacts.** (A–C) Alexa Fluor 546–phalloidin stain of actin and immunostain of Sec6 in a single cell (A), and at early (B) and compacted (C) contact between a pair of cells. Sec6 is localized to the cortical actin bundle in single cells, but as cells make early contacts, Sec6 begins to localize to the initial cell–cell contacts (B) and accumulates at cell–cell contacts in compacted cells (C). (D) MDCK cells stably expressing E-cadherin–tdRFP stained with syntaxin 4 antibodies showing that syntaxin 4 colocalized with E-cadherin at cell–cell contacts. Bar, 10 μm.

colocalized to initial cell–cell contacts and functioned there in the delivery of AQP3 from the Golgi to those contacts. In single MDCK cells, Sec6 and Sec8, two core components of the exocyst (TerBush et al., 1996), localized in the cytosol with the cortical actin bundle (Fig. 5 A). Upon initiation of cell–cell adhesion, Sec6 and Sec8 (not depicted) localized to the plasma membrane at sites of initial cell–cell adhesion, although some intracellular staining remained (Fig. 5 B). In compacted contacts between cells, Sec6 and Sec8 (not depicted) localized along the length of the cell–cell contact and at higher concentrations at the edges of the contact (Fig. 5 C), similar to the distribution of E-cadherin (Fig. 5 D). The basolateral SNARE syntaxin 4 localized to the lateral plasma membrane in polarized cells (Low et al., 1996) and in clusters at the plasma membrane in single cells. Syntaxin 4 also localized to initial cell–cell contacts (Fig. 5 D), and its distribution appeared to coincide with the distributions of E-cadherin (Fig. 5 D) and the exocyst (compare with Fig. 5, B and C). Thus, two components of the lateral targeting patch are recruited rapidly to the plasma membrane at cell–cell contacts after initiation of cell–cell adhesion.

We tested whether recruitment of components of the lateral targeting patch and microtubules were interdependent by examining their distribution after disruption or inhibition of each of the components. We initially tested whether localization of the exocyst and syntaxin 4 was microtubule dependent. MDCK cells stably expressing E-cadherin–tdRFP were plated in media containing 5 μM Ca^{2+} to inhibit cell–cell adhesion. Nocodazole was added to depolymerize microtubules (Fig. 6, A and B; and Fig. S1 A, available at http://www.jcb.org/cgi/content/full/jcb.200705094/DC1), and 1.8 mM Ca^{2+} was added to the media to initiate the formation of cell–cell contacts (Fig. 6, A and B; and Fig. S1 A). The disruption of microtubules did not impair the formation of cell–cell contacts as visualized by the distribution of E-cadherin (Fig. 6, A and B; and Fig. S1 A), nor the accumulation of Sec8 (Fig. 6 A) or syntaxin 4 (Fig. 6 B) at cell–cell contacts.

We next tested whether accumulation of the exocyst and SNARE complexes at forming cell–cell contacts was interdependent. The SNARE complex was disrupted in single cells by injecting tetanus toxin, which cleaves VAMP2 and VAMP3/cellubrevin (Fields et al., 2007), and protein distributions were examined after the addition of 1.8 mM Ca^{2+} to initiate cell–cell contact formation. Tetanus toxin did not disrupt contact formation, as visualized by E-cadherin localization at cell–cell contacts (Fig. 6, C and D; and Fig. S1 B), nor the accumulation of Sec8 (Fig. 6 C) or syntaxin 4 (Fig. 6 D) to the forming contact. Injection of function-blocking Sec8 antibodies, which caused Sec8 to relocalize from the cell–cell contact to the cytoplasm (Fig. S1 and Fig. S2, available at http://www.jcb.org/cgi/content/full/jcb.200705094/DC1), did not inhibit either E-cadherin–mediated cell–cell contact formation (Fig. 6 E and Fig. S1 C) or syntaxin 4 accumulation at cell–cell contacts (Fig. 6 E). Because both the Sec8 and syntaxin 4 antibodies are mouse monoclonals, we could not directly discriminate between the distributions of the two proteins by immunofluorescence microscopy in this experiment. However, the plasma membrane staining in Fig. 6 E is most likely syntaxin 4 staining, as microinjection of Sec8 antibodies

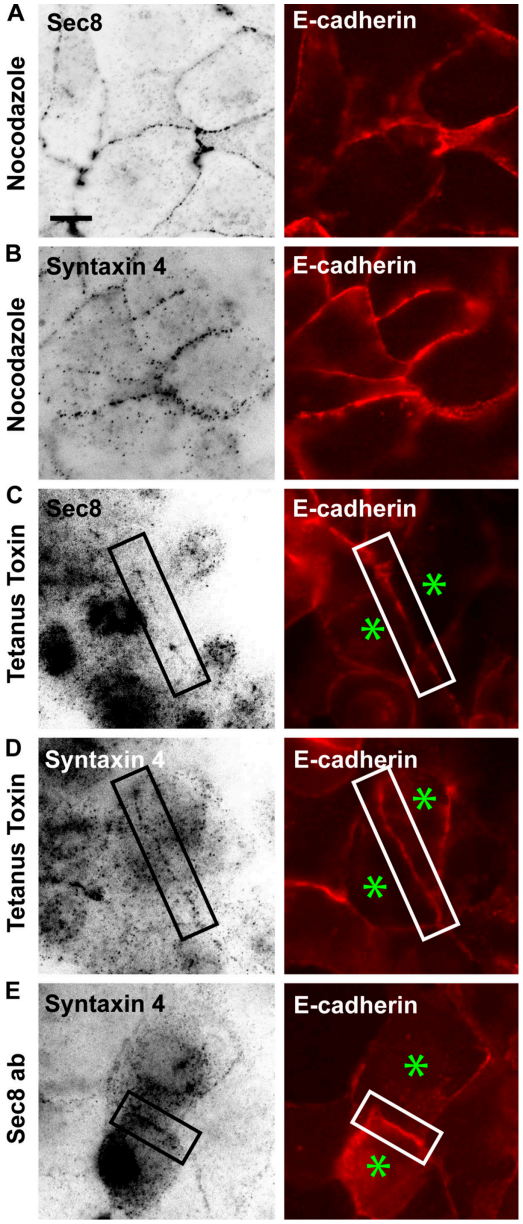

Figure 6. **Assembly of the lateral targeting patch at cell–cell contacts.** Single MDCK cells stably expressing E-cadherin–tdRFP were seeded in media containing 5 μM Ca^{2+} to inhibit cell–cell contact formation and were either incubated with nocodazole to depolymerize microtubules or were injected with tetanus toxin or function-blocking Sec8 antibodies. 1.8 mM Ca^{2+} was added to induce cell–cell contact formation, and cells were processed for immunofluorescence microscopy. (A and B) Cells were treated with nocodazole and immunostained for Sec8 (A) and syntaxin 4 (B). (C and D) Cells injected with tetanus toxin and immunostained for syntaxin 4 (C) and Sec8 (D). (E) Cells injected with Sec8 antibodies and immunostained for syntaxin 4. Cells indicated by asterisks were injected with tetanus toxin (C and D) or function-blocking Sec8 antibodies (E); note that pairs of injected cells were examined. (A–E) E-cadherin localized to cell–cell contacts after calcium readdition, and none of the treatments disrupted Sec8 or syntaxin 4 accumulation at cell–cell contacts. Bar, 10 μm.

caused all of the plasma membrane Sec8 to be redistributed into the cytoplasm (Fig. S1 C and Fig. S2). Thus, we conclude that the components of the lateral targeting patch (the exocyst and syntaxin 4) accumulate independently of each other and of microtubules at forming cell–cell contacts.

Functional inhibition of the exocyst or SNAREs blocks AQP3 delivery to the site of initial cell–cell adhesion

We next tested whether the lateral targeting patch was functional at the initial cell–cell contact by testing if disruption of different components interfered with delivery of AQP3 to sites of initial cell–cell contact. For this experiment, we chose to disrupt individual components with function-blocking antibodies or by toxin injection so that we could then directly and immediately assay the effects of loss of function on protein trafficking that had been temporarily blocked in and then released from the Golgi. This experimental design bypasses problems of long-term effects on cell–cell adhesion itself, as well as the nonselective pleiotropic effects on protein trafficking in general induced by knockdown of protein expression over a period of ∼36–48 h using siRNAs.

To investigate whether the exocyst plays a role in the delivery of AQP3 to the site of initial cell–cell adhesion, we injected cells forming cell–cell contacts with function-blocking Sec8 antibodies (Grindstaff et al., 1998b). We then synchronized exocytosis in the Golgi with the 19°C block and laser-activated trapped AQP3-PAGFP, as described in Materials and methods. Immunofluorescence of Sec8 antibody–injected cells showed that Sec8 was localized in the cytoplasm and not at cell–cell contacts (Fig. S1 C and Fig. S2). In contrast to noninjected cells (Fig. 7, A and E; Fig. 2 A; and Video 3, left) and cells injected with nonspecific IgG (Fig. S3, A and B; and Video 7, available at http://www.jcb.org/cgi/content/full/jcb.200705094/DC1), AQP3-PAGFP released from the Golgi in cells injected with Sec8 antibodies did not accumulate at sites of initial cell–cell contact (Fig. 7, D and E; and Video 8). Thus, inhibition of exocyst function at the plasma membrane was sufficient to block delivery of AQP3-PAGFP vesicles to cell–cell contacts even though syntaxin 4 localized to cell–cell contacts under these conditions (Fig. 5 E).

To test the involvement of the lateral membrane SNARE complex in AQP3-PAGFP vesicle fusion at sites of cell–cell contact, we injected cells with tetanus toxin. Results show that AQP3-PAGFP released from the Golgi did not accumulate at the cell–cell contact in cells injected with tetanus toxin (Fig. 7, C and E; and Video 9, available at http://www.jcb.org/cgi/content/full/jcb.200705094/DC1). Thus, the SNARE complex is also essential for the fusion of newly synthesized AQP3-PAGFP to sites of initial cell–cell contact. Collectively, these results demonstrate that the exocyst and t-SNAREs are rapidly and precisely recruited to cell–cell contacts, and that both complexes are required for AQP3 delivery and accumulation at initial sites of E-cadherin–mediated cell–cell adhesion.

Transport of AQP3 to the site of initial cell adhesion is microtubule dependent

Vesicles travel from the region of the Golgi via microtubules to the plasma membrane (Wacker et al., 1997) and to sites of established cell–cell contacts (Shaw et al., 2007). Although microtubules undergo a complex reorganization as epithelial cells polarize (Bacallao et al., 1989; Grindstaff et al., 1998a), microtubules in nonpolarized epithelial cells are initially organized in an

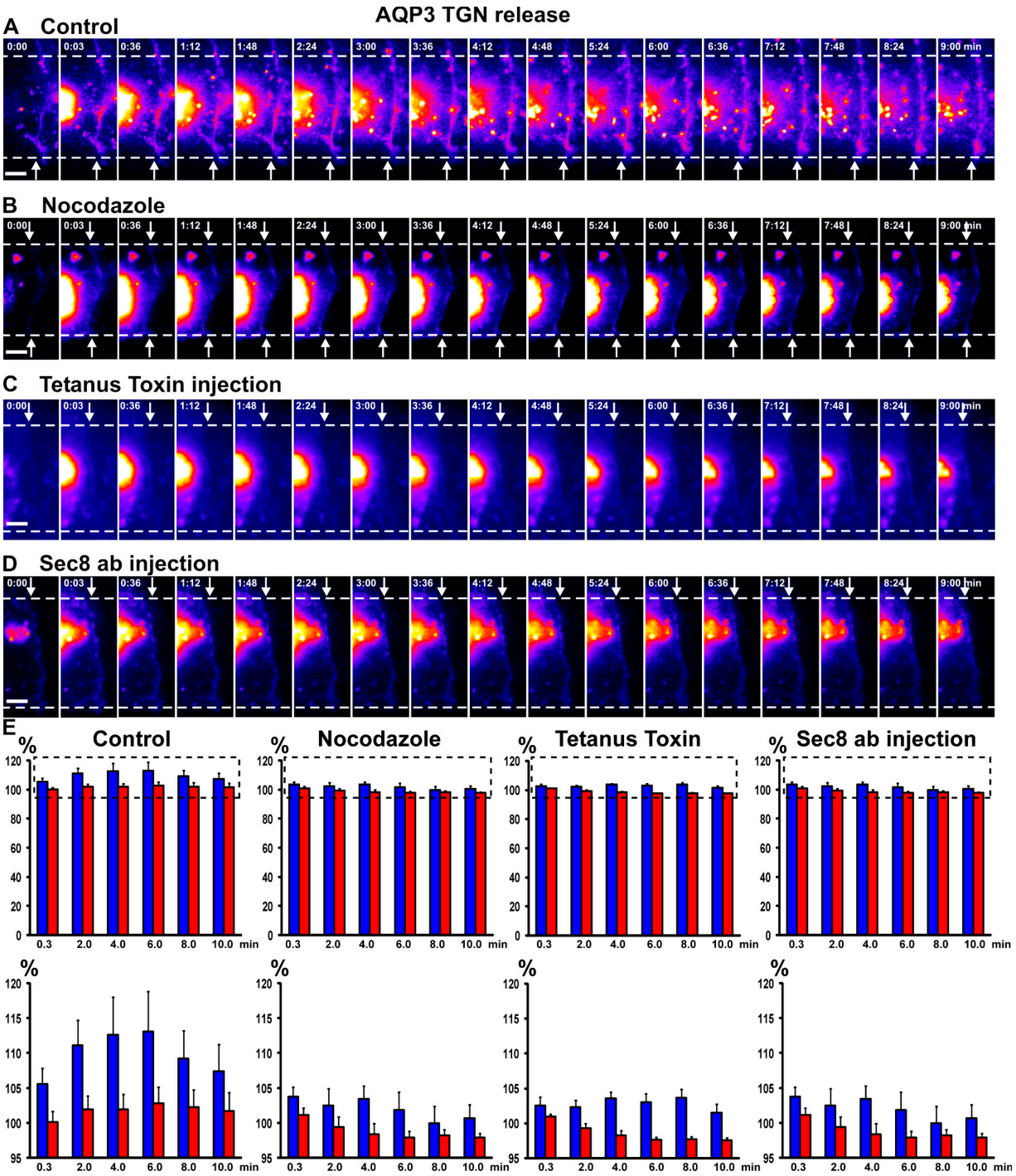

Figure 7. **Delivery of Golgi-accumulated AQP3-PAGFP to cell–cell contacts is blocked in the presence of nocodazole, Sec8 antibodies, or tetanus toxin.** (A–D) Representative examples of AQP3-PAGFP released from a 19°C block in the Golgi (control; A), in pairs of adhering cells treated with nocodazole (B), or microinjected with tetanus toxin (C) or Sec8 function-blocking antibodies (D). AQP3-PAGFP only accumulated at cell–cell contact in the control and not after inhibition of any one component of the lateral targeting patch. Arrows point to the edge of contact between two single cells, and numbers indicate the time (in minutes) after activation. The fluorescence intensity scale is pseudocolored. Bars, 5 µm. (E) Quantitation over time of a small spot of AQP3-PAGFP fluorescence at the cell–cell contact proximal to the Golgi. The dashed boxes (top) indicate the insets shown (bottom). Data points are averages of four to five independent experiments, and the error bars represent the SEM (blue, fluorescence intensity at cell–cell contacts; red, fluorescence intensity at the plasma membrane as equidistant from the Golgi as the spot measured at the cell–cell contact). Numbers indicate the time (in minutes) after activation. See Videos 8–10, available at http://www.jcb.org/cgi/content/full/jcb.200705094/DC1.

array similar to that in fibroblasts, in which they extend radially from the centrosome toward the periphery, where they impinge on initial E-cadherin–mediated contacts between cells (Ligon et al., 2001; Stehbens et al., 2006). We tested whether microtubules are important in the delivery of newly synthesized AQP3 from the Golgi to sites of initial cell–cell contact. AQP3-PAGFP

was accumulated in the Golgi at 19°C, and microtubules were depolymerized with nocodazole before the shift to 37°C and laser-activation of a small spot of AQP3-PAGFP in the Golgi in cells forming contacts; note that cell–cell contacts were not disrupted under these conditions (Fig. 6, A and B; and Fig. S1 A). We measured the fluorescence intensity of AQP3-PAGFP at the site of cell–cell contact and the noncontacting plasma membrane and did not detect an increase at either site (Fig. 7, B and E; and Video 10, available at http://www.jcb.org/cgi/content/full/jcb.200705094/DC1), indicating that, in the absence of microtubules, AQP3 was not transported from the Golgi region to the site of initial cell–cell adhesion, even though both the exocyst and SNARE complexes remained localized to cell–cell contacts.

Discussion

The establishment of cell surface polarity is common to many cell types and requires the accumulation of specific proteins in spatially restricted regions of the plasma membrane that uniquely contribute to cell and tissue functions (Yamada and Nelson, 2007). In transporting epithelia, the spatial segregation of proteins to the apical and basolateral membrane domains is the basis for the formation of ion and solute gradients across the epithelial monolayer (Rodriguez-Boulan et al., 2005). Similarly, the spatial restriction of subsets of proteins to neuronal (Hazuka et al., 1999; Waites et al., 2005) and immunological synapses (Taner et al., 2004; Hong, 2005) are critical to the functions of these cell types. Studies have shown that cell–cell adhesion coincides with the development of cell surface polarity in epithelia (Vega-Salas et al., 1987; Wang et al., 1990) and other cell types (Yamada and Nelson, 2007) and is required to maintain stem cell–niche interactions (Song et al., 2002; Yamashita et al., 2003) and the correct orientation of asymmetric stem cell divisions (Yamashita et al., 2003; Lechler and Fuchs, 2005; Siegrist and Doe, 2006; Chang et al., 2007). Important problems are to identify how these spatial cues initiate formation of these cell surface domains, and the downstream machinery that regulates the type of protein that is delivered to and integrated into the membrane domain.

Polarized transporting epithelia provide a useful system to approach these problems, because the mechanisms involved in protein sorting have been well described, and cell–cell adhesion can be easily manipulated and imaged. Apical and basolateral membrane proteins appear to be constitutively sorted from each other in the Golgi and/or recycling endosome (Yoshimori et al., 1996; Ang et al., 2004), whereas their distributions are intermixed at the plasma membrane in nonpolarized cells (Wang et al., 1990; Yoshimori et al., 1996). E-cadherin–mediated cell–cell adhesion appears to provide a spatial cue for cells to distinguish an unbounded (apical) from a bounded (basolateral) surface and to accumulate apical and basolateral membrane proteins in the correct surface (Wang et al., 1990), but the mechanisms linking E-cadherin to protein sorting and redistribution to different plasma membrane domains are unknown.

To test the role of E-cadherin–mediated cell–cell adhesion in protein trafficking and cell surface distribution, we took a direct approach by imaging the delivery of two highly homologous apical (AQP5) and basolateral (AQP3) membrane proteins to sites of initial cell–cell adhesion. Because apical and basolateral proteins are presorted before their arrival at the cell surface (Rodriguez-Boulan et al., 2005), including AQPs (Wellner et al., 2005; Rai et al., 2006), we could ask whether plasma membrane sites at the earliest stages of cell–cell adhesion become specialized for the delivery of basolateral rather than apical vesicles and, if so, investigate the nature of the cellular machinery involved.

Newly synthesized AQP3 localized with E-cadherin at initial cell–cell contacts

E-cadherin dynamics and the formation of initial cell–cell contacts are well described in MDCK cells (Adams et al., 1998; Ehrlich et al., 2002). When we compared the distribution of E-cadherin at such contacts with those of AQP3 and AQP5, we found that after a short delay of a few minutes the basolateral AQP3, but not the homologous apical AQP5, accumulated rapidly at cell–cell contacts in a distribution that was identical to that of E-cadherin.

We directly tested whether AQP3 and AQP5 were delivered directly to the site of cell–cell contact by following a pool of photoactivated AQP3-PAGFP and AQP5-PAGFP that had accumulated in the Golgi because of a temperature block (Pfeiffer et al., 1985). We observed directly that AQP3, but not AQP5, was rapidly delivered to the forming cell–cell contact. In addition, we detected little or no increase in AQP3-PAGFP at the noncontacting membrane, indicating that AQP3 was directly targeted to and immediately integrated into the forming cell–cell contact. Note that we could confirm AQP3-containing post-Golgi carriers originating in the Golgi region that moved rapidly in linear pathways at speeds averaging 0.2–0.3 μm/s through the cytoplasm and disappeared at the forming cell–cell contact; it is likely that AQP3 vesicles are transported on microtubules, because this speed is similar to that generated by kinesin, and microtubules are required for AQP3 delivery. A recent study reported that the gap junction protein Cx43 is also delivered along microtubules to established sites of E-cadherin–mediated cell–cell contacts (Johnson et al., 2002; Shaw et al., 2007).

Establishment of a functional lateral targeting patch upon initial cell–cell adhesion

Because AQP3 but not AQP5 was delivered to cell–cell contacts, we directly tested whether a targeting patch specific for basolateral vesicles is assembled upon E-cadherin–mediated cell–cell adhesion. Our data indicate that microtubules, the exocyst, and t-SNAREs are essential components of this lateral targeting patch. We showed that the exocyst and the t-SNARE syntaxin 4 colocalized with E-cadherin at early cell–cell contacts, and it has been shown by others that microtubule plus ends extend radially into cell–cell contacts (Stehbens et al., 2006; Shaw et al., 2007). Functional disruption of any one of these components did not interfere with the establishment of cell–cell adhesion or the localization of other components to cell–cell contact. Because there is a large amount of E-cadherin on the cell surface before cell adhesion (Adams et al. 1998), it is therefore likely that initial cell–cell adhesion does not require the delivery of E-cadherin from intracellular compartments. However,

functional disruption of any one of these components blocked delivery of AQP3 to sites of cell–cell contact, indicating that they are all essential for separate stages in vesicle delivery (microtubules), tethering (the exocyst), and fusion (SNAREs) with the plasma membrane at cell–cell contacts.

At present we do not know how AQP5 is sorted to the apical plasma membrane in these cells. Studies in salivary glands indicate a role for lipid rafts in AQP5 delivery (Ishikawa et al., 2005), and lipid rafts are thought to be involved in targeting proteins to the apical membrane of MDCK cells (Schuck and Simons, 2004; Paladino et al., 2006). However, it is also possible that the basolateral targeting patch is selective for the type of vesicle that can fuse with the membrane by excluding apical (AQP5) but accepting basolateral (AQP3) vesicles. Indeed, function-blocking Sec8 antibodies inhibit basal-lateral (low density lipoprotein receptor; Grindstaff et al., 1998b) and AQP3 (this study) but not apical (p75; Grindstaff et al., 1998b) protein delivery to the plasma membrane; in addition, we occasionally observed that AQP5 localized to adhesion sites at the onset of contact formation but then rapidly disappeared as the contact expanded. Thus, the segregation of apical and basolateral membrane proteins may involve two independent sorting sites and mechanisms, one in the Golgi involving the recognition of intrinsic sorting signals on proteins (Rodriguez-Boulan and Musch, 2005) and the other at the plasma membrane involving vesicle recognition by the lateral targeting patch, which together ensure the accumulation of specific proteins in the correct membrane domain.

Recruitment of microtubules and the exocyst to sites of cell–cell contact may be through interactions with the E-cadherin complex. Microtubules interact with dynein, which is localized to cell–cell contacts and may bind the cadherin–catenin complex (Ligon et al., 2001; Shaw et al., 2007). Components of the plasma membrane exocyst complex can be cross-linked in a complex with E-cadherin and nectin 2α (Yeaman et al., 2004), indicating that E-cadherin accumulation during cell–cell adhesion corecruits the exocyst. However, we do not know if the exocyst complex at the plasma membrane is complete or composes a partial complex that is completed by additional components on basolateral vesicles (Yeaman et al., 2001; Folsch et al., 2003). Mechanisms involved in the accumulation of t-SNARE complexes to the basolateral membrane domain are not understood, although recent studies indicate that apical and basolateral t-SNAREs are in separate microdomains in the plasma membrane in single cells (Low et al., 2006), and a sorting signal has been identified on the apical syntaxin 3 (Sharma et al., 2006); whether basolateral t-SNAREs (syntaxin 4) are segregated and accumulate with E-cadherin is not known.

In addition to direct mechanisms regulating vesicle delivery to the sites of cell–cell contacts, it is thought that a complex of proteins including Scribble, the partitioning defective complex, and lethal giant larva are involved in determining the apico-basal axis of polarity in epithelial cells (Roh and Margolis, 2003; Macara, 2004) . It is possible that these protein complexes are recruited to cell–cell contacts and regulate the organization and maintenance of the boundary between apical and basolateral membranes at later stages of polarization.

In summary, our results provide the first direct experimental evidence for a mechanistic link between E-cadherin–mediated cell–cell contact, directed protein sorting, and the initiation of membrane domain organization. E-cadherin contacts orient microtubules for direct vesicle delivery from the Golgi and rapidly recruit a targeting patch that selectively tethers (the exocyst) and fuses (t-SNARE) basolateral vesicles to the cell–cell contact and may exclude apical vesicles from those sites. Given that these components of the epithelial lateral targeting patch are widely expressed in diverse cell types, this mechanism may be involved in establishing membrane domains in other polarized cells.

Materials and methods

Constructs and stable cell lines

E-cadherin–tdRFP was generated from EGFP-tagged E-cadherin (Adams et al., 1998). Photoactivatable constructs were generated by subcloning PAGFP (a gift from J. Lippincott-Schwartz, National Institutes of Health, Bethesda, MD) from the N1 vector (CLONTECH Laboratories, Inc.) into AQP3-EGFP–N2 and AQP5-EGFP–N2 (gifts from A. Aperia, Karolinska Institutet, Stockholm, Sweden; Zelenina et al., 2003) using BSeRI. MDCK GII cells were transfected with Effectene (QIAGEN) and selected with G418 (Invitrogen). Cells stably expressing E-cadherin–tdRFP (a gift from S. Yamada, University of California, Davis, Davis, CA) were transfected with AQP3-EGFP and subjected to four rounds of FACS to generate cells stably expressing both E-cadherin–tdRFP and AQP3-EGFP. Cells stably expressing E-cadherin–tdRFP were transiently transfected with AQP5-EGFP to generate double-expressing cells. All constructs were stably expressed in MDCK GII cells without any apparent change in phenotype. Correct localization was verified by the imaging (see the following section) of cells grown on filters for 10 d.

Microscopy

Cells were seeded on collagen-coated coverslips and allowed to attach and spread for at least 1 h before imaging. Time-lapse imaging was performed in phenol red–free DME media (Sigma-Aldrich) with 10% fetal bovine serum (Atlas Biologicals) and 25 mM Hepes (Invitrogen) using the Marianas system (Intelligent Imaging Innovations) with a microscope (Axiovert 200M; Carl Zeiss MicroImaging, Inc.) equipped with a camera (Photometrics CoolSNAP; Roper Scientific), a laser system (MicroPoint FRAP; Photonic Instruments, Inc.), and a TIRF system (TIRF Slider; Carl Zeiss MicroImaging, Inc.). An α Plan-FLUAR 1.45 oil (for TIRF) and a 100× Plan-APOCHROMAT 1.40 oil differential interference contrast (for epifluorescence) objectives were used (both obtained from Carl Zeiss MicroImaging, Inc.). Images were analyzed using Slidebook (Intelligent Imaging Innovations) or ImageJ (available at http://rsb.info.nih.gov/ij) software. For initial cell adhesion, cells starting to form contact were imaged every minute for 5 h.

For direct delivery to the forming contact, newly synthesized proteins were accumulated in the Golgi by a 19°C block for 3 h in the presence of 0.02 μg/ml cyclohexamide. Cells were warmed on the microscope stage to 37°C for 15 min before imaging. Imaging was performed every 3 s for 10 min, and a maximum of six movies was obtained. After the first frame, the movie was paused, and a region covering the Golgi was activated using the Micropoint FRAP laser system. For microtubule depolymerization, 33 μM nocodazole was added for the last 30 min of the 19°C block, and injections were performed as described in the following section. A small spot at the contacting plasma membranes was quantified before activation, just after activation, and at 2, 4, 6, 8, and 10 (9 min 57 s) min after the start of the time lapse. The fluorescent signal was normalized to the frame before activation.

To measure the half-time of intensity recovery, AQP3-PAGFP cells were plated 24 h (forming monolayers) or 1 h (initial contacts) before analysis. Cells were imaged every 3 s for 10 min. After the first frame, the time lapse was paused, and a small area of the contact was activated. The intensity profiles were analyzed for the maximum intensity recovery (percentage) and fitted to a single exponential function up to 10 min after photoactivation to extract the half time of intensity recovery ($t_{1/2}$).

To measure diffusion out of the contact, AQP3-EGFP cells were mixed with MDCK GII cells. Pairs of cells consisting of one expressing and one nonexpressing cell were analyzed. 0.02 μg/ml cyclohexamide was added to eliminate delivery of newly synthesized protein to the contact

during analysis. A spot of the plasma membrane adjacent to the contacting plasma membranes was continuously photobleached for 30 min. A small area of the contacting membranes was quantified before and then every 3 min. Values were background subtracted and normalized to the frame just before photobleaching.

For assessment of adhesion after treatments, single cells expressing E-cadherin–tdRFP were plated in low calcium media containing 5 μM Ca^{2+} to inhibit cell–cell adhesion, and different manipulations (nocodazole treatment, tetanus toxin, or Sec8 antibody injection; see the following section) were performed on single cells; 1.8 mM Ca^{2+} was added back to the growth medium to initiate cell–cell adhesion, and the amount of E-cadherin at cell–cell adhesion was examined. 33 μM nocodazole was added for the last 30 min before calcium readdition.

Microinjection

Sec8 antibodies (equal mixture of 2E9, 2E12, 5C3, 10C2, and 17A10 hybridoma supernatants; Yeaman et al., 2001) were concentrated 16 times on a column (Microcon 50.000 MW; Millipore) and washed 5 times with microinjection buffer (10 mM Hepes, 140 mM KCl [pH 7.4]). The mixture was diluted five times for injection into microinjection buffer. 60 ng/μl tetanus toxin (needle concentration; List Biological Laboratories, Inc.), Sec8 antibodies, and 1 mg/ml rabbit IgG (needle concentration) were microinjected into one cell of a duplet using a microinjection system (Eppendorf). 0.5–1 mg/ml Texas red or FITC-labeled dextran were coinjected to identify injected cells. Newly synthesized protein was accumulated at the Golgi, released, and imaged as described in the previous section. After imaging, Sec8 antibody–injected cells were fixed, permeabilized, and stained with secondary goat anti–mouse Cy5-conjugated antibody.

Immunostaining

Cells were seeded on collagen-coated coverslips for 1 h at subconfluent density, fixed in 2% paraformaldehyde, and permeabilized with Triton X-100. For staining of microtubules, cells were fixed in ice-cold methanol at −20°C. Primary antibodies were as follows: monoclonal Sec6 (clone 9H5) and Sec8 (clone 8F12; Hsu et al., 1996), Syntaxin 4 (BD Biosciences), DM1α tubulin (Sigma-Aldrich), Gp135 3F2/D8 (a gift from G.K. Ojakian, State University of New York Health Science Center, Brooklyn, NY), and polyclonal NaK-ATPase (a3NKA; Nelson and Veshnock, 1986) and ZO1 (Zymed Laboratories).

Fluorescence microscopy of fixed specimens

Images were obtained using the Marianas system, except for AQP5-EGFP images, which were obtained with a microscope (model IX-70; Olympus). The AQP5-EGFP images were processed using deconvolution software (DeltaVision; Applied Precision) on a workstation (Silicon Graphics, Inc.).

Online supplemental material

Fig. S1 depicts E-cadherin localization in adhering cells after a change in media containing 5 μM Ca^{2+} to 1.8 mM Ca^{2+} in the presence of nocodazole (A), tetanus toxin (B), or Sec8 function-blocking antibody (C). Fig. S2 shows a retrospective stain of Sec8 localization after Sec8 antibody injection. Fig. S3 depicts the distribution of Golgi-accumulated AQP3-PAGFP released from the Golgi after a shift in temperature from 19°C to 37°C in the presence of rabbit IgG. Video 1 provides a time-lapse movie of two single cells making initial cell–cell contact. The cells are stably expressing AQP3-EGFP (green) and E-cadherin–tdRFP (red). Video 2 shows a time-lapse movie of two single cells making initial cell–cell contact. The cells are transiently expressing AQP5-EGFP (green) and stably expressing E-cadherin–tdRFP (red). Video 3 provides a time-lapse movie of cell pairs stably expressing AQP3-PAGFP (left) and AQP5-PAGFP (right) after release from a 19°C temperature block. AQP3-PAGFP and AQP5-PAGFP were photoactivated in the Golgi region, and images were captured every 3 s for 10 min. Video 4 shows a time-lapse movie of a cell pair stably expressing AQP3-PAGFP after release from a 19°C temperature block. AQP3-PAGFP was photoactivated in the Golgi region, and images were captured every 3 s. Video 5 provides a time-lapse movie using TIRF microscopy of a cell pair stably expressing AQP3-PAGFP after release from a 19°C temperature block. Video 6 shows a time-lapse movie of a cell pair stably expressing AQP3-PAGFP. Cells that had formed confluent monolayers over a 24-h time period are shown on the left, and initial cell–cell contact is shown on the right. AQP3-PAGFP was photoactivated at a small point within the cell–cell contact. Video 7 provides a time-lapse movie of a cell pair stably expressing AQP3-PAGFP after release from a 19°C temperature block. One cell was injected with rabbit IgG before a 19°C temperature block. Video 8 shows a time-lapse movie of a cell pair stably expressing AQP3-PAGFP after release from a 19°C temperature block. One cell was injected with Sec8 antibodies before a 19°C temperature block. Video 9 provides a time-lapse movie of a cell pair stably expressing AQP3-PAGFP after release from a 19°C temperature block. One cell was injected with tetanus toxin before a 19°C temperature block. Video 10 shows a time-lapse movie of a cell pair stably expressing AQP3-PAGFP after release from a 19°C temperature block. Cells were treated with nocodazole during the last 30 min of a 19°C temperature block. Online supplemental material is available at http://www.jcb.org/cgi/content/full/jcb.200705094/DC1.

We thank Dr. Anita Aperia for the AQP3-EGFP and AQP5-EGFP constructs, Dr. George Ojakian for the anti-gp135 hybridoma, Dr. Jennifer Lippincott-Schwartz for PAGFP, and Dr. Soichiro Yamada for invaluable help and discussions and for the cell line stably expressing tdRFP-linked E-cadherin. We thank Laura Edgington for technical support and Dr. Erik Meijering for the MTrackJ program.

This work was supported by National Institutes of Health grant R01 GM35527 (to W.J. Nelson) and a postdoctoral fellowship from the Danish Medical Research Foundation (to L.N. Nejsum).

Submitted: 16 May 2007
Accepted: 15 June 2007

References

Adams, C.L., Y.T. Chen, S.J. Smith, and W.J. Nelson. 1998. Mechanisms of epithelial cell–cell adhesion and cell compaction revealed by high-resolution tracking of E-cadherin–green fluorescent protein. *J. Cell Biol.* 142:1105–1119.

Ang, A.L., T. Taguchi, S. Francis, H. Folsch, L.J. Murrells, M. Pypaert, G. Warren, and I. Mellman. 2004. Recycling endosomes can serve as intermediates during transport from the Golgi to the plasma membrane of MDCK cells. *J. Cell Biol.* 167:531–543.

Bacallao, R., C. Antony, C. Dotti, E. Karsenti, E.H. Stelzer, and K. Simons. 1989. The subcellular organization of Madin-Darby canine kidney cells during the formation of a polarized epithelium. *J. Cell Biol.* 109:2817–2832.

Brunger, A.T. 2005. Structure and function of SNARE and SNARE-interacting proteins. *Q. Rev. Biophys.* 38:1–47.

Chang, J.T., V.R. Palanivel, I. Kinjyo, F. Schambach, A.M. Intlekofer, A. Banerjee, S.A. Longworth, K.E. Vinup, P. Mrass, J. Oliaro, et al. 2007. Asymmetric T lymphocyte division in the initiation of adaptive immune responses. *Science*. 315:1687–1691.

Chen, Y.A., and R.H. Scheller. 2001. SNARE-mediated membrane fusion. *Nat. Rev. Mol. Cell Biol.* 2:98–106.

Drubin, D.G., and W.J. Nelson. 1996. Origins of cell polarity. *Cell*. 84:335–344.

Ehrlich, J.S., M.D. Hansen, and W.J. Nelson. 2002. Spatio-temporal regulation of Rac1 localization and lamellipodia dynamics during epithelial cell-cell adhesion. *Dev. Cell*. 3:259–270.

Fields, I.C., E. Shteyn, M. Pypaert, V. Proux-Gillardeaux, R.S. Kang, T. Galli, and H. Folsch. 2007. v-SNARE cellubrevin is required for basolateral sorting of AP-1B–dependent cargo in polarized epithelial cells. *J. Cell Biol.* 177:477–488.

Folsch, H., M. Pypaert, S. Maday, L. Pelletier, and I. Mellman. 2003. The AP-1A and AP-1B clathrin adaptor complexes define biochemically and functionally distinct membrane domains. *J. Cell Biol.* 163:351–362.

Frigeri, A., M.A. Gropper, C.W. Turck, and A.S. Verkman. 1995. Immunolocalization of the mercurial-insensitive water channel and glycerol intrinsic protein in epithelial cell plasma membranes. *Proc. Natl. Acad. Sci. USA*. 92:4328–4331.

Grindstaff, K.K., R.L. Bacallao, and W.J. Nelson. 1998a. Apiconuclear organization of microtubules does not specify protein delivery from the trans-Golgi network to different membrane domains in polarized epithelial cells. *Mol. Biol. Cell*. 9:685–699.

Grindstaff, K.K., C. Yeaman, N. Anandasabapathy, S.C. Hsu, E. Rodriguez-Boulan, R.H. Scheller, and W.J. Nelson. 1998b. Sec6/8 complex is recruited to cell-cell contacts and specifies transport vesicle delivery to the basal-lateral membrane in epithelial cells. *Cell*. 93:731–740.

Guo, W., and P. Novick. 2004. The exocyst meets the translocon: a regulatory circuit for secretion and protein synthesis? *Trends Cell Biol.* 14:61–63.

Hazuka, C.D., D.L. Foletti, S.C. Hsu, Y. Kee, F.W. Hopf, and R.H. Scheller. 1999. The sec6/8 complex is located at neurite outgrowth and axonal synapse-assembly domains. *J. Neurosci.* 19:1324–1334.

He, X., C.M. Tse, M. Donowitz, S.L. Alper, S.E. Gabriel, and B.J. Baum. 1997. Polarized distribution of key membrane transport proteins in the rat submandibular gland. *Pflugers Arch.* 433:260–268.

Hong, W. 2005. Cytotoxic T lymphocyte exocytosis: bring on the SNAREs! *Trends Cell Biol.* 15:644–650.

Hsu, S.C., A.E. Ting, C.D. Hazuka, S. Davanger, J.W. Kenny, Y. Kee, and R.H. Scheller. 1996. The mammalian brain rsec6/8 complex. *Neuron*. 17:1209–1219.

Hua, W., E.C. Young, M.L. Fleming, and J. Gelles. 1997. Coupling of kinesin steps to ATP hydrolysis. *Nature*. 388:390–393.

Ikonen, E., M. Tagaya, O. Ullrich, C. Montecucco, and K. Simons. 1995. Different requirements for NSF, SNAP, and Rab proteins in apical and basolateral transport in MDCK cells. *Cell*. 81:571–580.

Ishikawa, Y., Z. Yuan, N. Inoue, M.T. Skowronski, Y. Nakae, M. Shono, G. Cho, M. Yasui, P. Agre, and S. Nielsen. 2005. Identification of AQP5 in lipid rafts and its translocation to apical membranes by activation of M3 mAChRs in interlobular ducts of rat parotid gland. *Am. J. Physiol. Cell Physiol.* 289:C1303–C1311.

Johnson, R.G., R.A. Meyer, X.R. Li, D.M. Preus, L. Tan, H. Grunenwald, A.F. Paulson, D.W. Laird, and J.D. Sheridan. 2002. Gap junctions assemble in the presence of cytoskeletal inhibitors, but enhanced assembly requires microtubules. *Exp. Cell Res.* 275:67–80.

Lechler, T., and E. Fuchs. 2005. Asymmetric cell divisions promote stratification and differentiation of mammalian skin. *Nature*. 437:275–280.

Li, X., S.H. Low, M. Miura, and T. Weimbs. 2002. SNARE expression and localization in renal epithelial cells suggest mechanism for variability of trafficking phenotypes. *Am. J. Physiol. Renal Physiol.* 283:F1111–F1122.

Ligon, L.A., S. Karki, M. Tokito, and E.L. Holzbaur. 2001. Dynein binds to beta-catenin and may tether microtubules at adherens junctions. *Nat. Cell Biol.* 3:913–917.

Low, S.H., S.J. Chapin, T. Weimbs, L.G. Komuves, M.K. Bennett, and K.E. Mostov. 1996. Differential localization of syntaxin isoforms in polarized Madin-Darby canine kidney cells. *Mol. Biol. Cell*. 7:2007–2018.

Low, S.H., A. Vasanji, J. Nanduri, M. He, N. Sharma, M. Koo, J. Drazba, and T. Weimbs. 2006. Syntaxins 3 and 4 are concentrated in separate clusters on the plasma membrane before the establishment of cell polarity. *Mol. Biol. Cell*. 17:977–989.

Macara, I.G. 2004. Parsing the polarity code. *Nat. Rev. Mol. Cell Biol.* 5:220–231.

McNeill, H., M. Ozawa, R. Kemler, and W.J. Nelson. 1990. Novel function of the cell adhesion molecule uvomorulin as an inducer of cell surface polarity. *Cell*. 62:309–316.

Nejsum, L.N., T.H. Kwon, U.B. Jensen, O. Fumagalli, J. Frokiaer, C.M. Krane, A.G. Menon, L.S. King, P.C. Agre, and S. Nielsen. 2002. Functional requirement of aquaporin-5 in plasma membranes of sweat glands. *Proc. Natl. Acad. Sci. USA*. 99:511–516.

Nelson, W.J., and P.J. Veshnock. 1986. Dynamics of membrane-skeleton (fodrin) organization during development of polarity in Madin-Darby canine kidney epithelial cells. *J. Cell Biol.* 103:1751–1765.

O'Brien, L.E., T.S. Jou, A.L. Pollack, Q. Zhang, S.H. Hansen, P. Yurchenco, and K.E. Mostov. 2001. Rac1 orientates epithelial apical polarity through effects on basolateral laminin assembly. *Nat. Cell Biol.* 3:831–838.

Paladino, S., T. Pocard, M.A. Catino, and C. Zurzolo. 2006. GPI-anchored proteins are directly targeted to the apical surface in fully polarized MDCK cells. *J. Cell Biol.* 172:1023–1034.

Pfeiffer, S., S.D. Fuller, and K. Simons. 1985. Intracellular sorting and basolateral appearance of the G protein of vesicular stomatitis virus in Madin-Darby canine kidney cells. *J. Cell Biol.* 101:470–476.

Rai, T., S. Sasaki, and S. Uchida. 2006. Polarized trafficking of the aquaporin-3 water channel is mediated by an NH2-terminal sorting signal. *Am. J. Physiol. Cell Physiol.* 290:C298–C304.

Rodriguez-Boulan, E., G. Kreitzer, and A. Musch. 2005. Organization of vesicular trafficking in epithelia. *Nat. Rev. Mol. Cell Biol.* 6:233–247.

Rodriguez-Boulan, E., and A. Musch. 2005. Protein sorting in the Golgi complex: shifting paradigms. *Biochim. Biophys. Acta*. 1744:455–464.

Roh, M.H., and B. Margolis. 2003. Composition and function of PDZ protein complexes during cell polarization. *Am. J. Physiol. Renal Physiol.* 285: F377–F387.

Schuck, S., and K. Simons. 2004. Polarized sorting in epithelial cells: raft clustering and the biogenesis of the apical membrane. *J. Cell Sci.* 117:5955–5964.

Sharma, N., S.H. Low, S. Misra, B. Pallavi, and T. Weimbs. 2006. Apical targeting of syntaxin 3 is essential for epithelial cell polarity. *J. Cell Biol.* 173:937–948.

Shaw, R.M., A.J. Fay, M.A. Puthenveedu, M. von Zastrow, Y.N. Jan, and L.Y. Jan. 2007. Microtubule plus-end-tracking proteins target gap junctions directly from the cell interior to adherens junctions. *Cell*. 128:547–560.

Siegrist, S.E., and C.Q. Doe. 2006. Extrinsic cues orient the cell division axis in *Drosophila* embryonic neuroblasts. *Development*. 133:529–536.

Song, X., C.H. Zhu, C. Doan, and T. Xie. 2002. Germline stem cells anchored by adherens junctions in the *Drosophila* ovary niches. *Science*. 296:1855–1857.

Stehbens, S.J., A.D. Paterson, M.S. Crampton, A.M. Shewan, C. Ferguson, A. Akhmanova, R.G. Parton, and A.S. Yap. 2006. Dynamic microtubules regulate the local concentration of E-cadherin at cell-cell contacts. *J. Cell Sci.* 119:1801–1811.

Streuli, C.H., N. Bailey, and M.J. Bissell. 1991. Control of mammary epithelial differentiation: basement membrane induces tissue-specific gene expression in the absence of cell–cell interaction and morphological polarity. *J. Cell Biol.* 115:1383–1395.

Taner, S.B., B. Onfelt, N.J. Pirinen, F.E. McCann, A.I. Magee, and D.M. Davis. 2004. Control of immune responses by trafficking cell surface proteins, vesicles and lipid rafts to and from the immunological synapse. *Traffic*. 5:651–661.

TerBush, D.R., T. Maurice, D. Roth, and P. Novick. 1996. The Exocyst is a multiprotein complex required for exocytosis in *Saccharomyces cerevisiae*. *EMBO J.* 15:6483–6494.

Vega-Salas, D.E., P.J. Salas, D. Gundersen, and E. Rodriguez-Boulan. 1987. Formation of the apical pole of epithelial (Madin-Darby canine kidney) cells: polarity of an apical protein is independent of tight junctions while segregation of a basolateral marker requires cell–cell interactions. *J. Cell Biol.* 104:905–916.

Wacker, I., C. Kaether, A. Kromer, A. Migala, W. Almers, and H.H. Gerdes. 1997. Microtubule-dependent transport of secretory vesicles visualized in real time with a GFP-tagged secretory protein. *J. Cell Sci.* 110:1453–1463.

Waites, C.L., A.M. Craig, and C.C. Garner. 2005. Mechanisms of vertebrate synaptogenesis. *Annu. Rev. Neurosci.* 28:251–274.

Wang, A.Z., G.K. Ojakian, and W.J. Nelson. 1990. Steps in the morphogenesis of a polarized epithelium. I. Uncoupling the roles of cell-cell and cell-substratum contact in establishing plasma membrane polarity in multicellular epithelial (MDCK) cysts. *J. Cell Sci.* 95:137–151.

Wellner, R.B., S. Hong, A.P. Cotrim, W.D. Swaim, and B.J. Baum. 2005. Modifying the NH2 and COOH termini of aquaporin-5: effects on localization in polarized epithelial cells. *Tissue Eng.* 11:1449–1458.

Yamada, S., and W.J. Nelson. 2007. Synapses: Sites of Cell Recognition, Adhesion, and Functional Specification. *Annu. Rev. Biochem.* 76:267–294.

Yamashita, Y.M., D.L. Jones, and M.T. Fuller. 2003. Orientation of asymmetric stem cell division by the APC tumor suppressor and centrosome. *Science*. 301:1547–1550.

Yeaman, C., K.K. Grindstaff, J.R. Wright, and W.J. Nelson. 2001. Sec6/8 complexes on trans-Golgi network and plasma membrane regulate late stages of exocytosis in mammalian cells. *J. Cell Biol.* 155:593–604.

Yeaman, C., K.K. Grindstaff, and W.J. Nelson. 2004. Mechanism of recruiting Sec6/8 (exocyst) complex to the apical junctional complex during polarization of epithelial cells. *J. Cell Sci.* 117:559–570.

Yoshimori, T., P. Keller, M.G. Roth, and K. Simons. 1996. Different biosynthetic transport routes to the plasma membrane in BHK and CHO cells. *J. Cell Biol.* 133:247–256.

Zelenina, M., A.A. Bondar, S. Zelenin, and A. Aperia. 2003. Nickel and extracellular acidification inhibit the water permeability of human aquaporin-3 in lung epithelial cells. *J. Biol. Chem.* 278:30037–30043.